Contents lists available at ScienceDirect

Deep-Sea Research Part II

Nitrous oxide in the northern Gulf of Aqaba and the central Red Sea

Hermann W. Bange[a,*], Annette Kock[a], Nicole Pelz[a], Mark Schmidt[a], Florian Schütte[a], Sylvia Walter[a,b], Anton F. Post[c,d], Burton H. Jones[e], Benjamin Kürten[e,f]

[a] GEOMAR Helmholtz Centre for Ocean Research Kiel, Kiel, Germany
[b] Now at Institute for Marine and Atmospheric Research (IMAU), Utrecht University, Utrecht, the Netherlands
[c] Interuniversity Institute for Marine Sciences, Eilat, Israel
[d] Now at Division of Research, Florida Atlantic University, Boca Raton, FL, USA
[e] King Abdullah University of Science and Technology (KAUST), Red Sea Research Center (RSRC), Biological and Environmental Sciences & Engineering Division (BESE), Thuwal, Saudi Arabia
[f] Project Management Jülich, Jülich Research Centre GmbH, Rostock, Germany

ARTICLE INFO

ABSTRACT

Nitrous oxide (N_2O) is a climate-relevant atmospheric trace gas. It is produced as an intermediate of the nitrogen cycle. The open and coastal oceans are major sources of atmospheric N_2O. However, its oceanic distribution is still largely unknown. Here we present the first measurements of the water column distribution of N_2O in the Gulf of Aqaba and the Red Sea. Samples for N_2O depth profiles were collected at the time-series site Station A in the northern Gulf of Aqaba (June and September 2003, and February 2004) and at several stations in the central Red Sea (October 2014, January and August 2016). Additionally, we measured N_2O concentrations in brine pool samples collected in the northern and central Red Sea (January 2005 and August 2016). In the Gulf of Aqaba, N_2O surface concentrations ranged from 6 to 8 nmol L^{-1} (97–111% saturation) and were close to the equilibrium with the overlying atmosphere. A pronounced temporal variability of the N_2O water column distribution was observed. We suggest that this variability is a reflection of the interplay between N_2O production by nitrification and its consumption by N_2 fixation in the layers below 150 m during summer. N_2O surface concentrations and saturations in the central Red Sea basin ranged from 2 to 9 nmol L^{-1} (43–155% saturation). A pronounced temporal variability with significant supersaturation in October 2014 and undersaturation in January and August 2016 was observed in the surface layer. In October 2014, N_2O in the water column seemed to result from production via nitrification. Low N_2O water column concentrations in January and August 2016 indicated a significant removal of N_2O. We speculate that either in-situ consumption or remote loss processes of N_2O such as denitrification in coastal regions were responsible for this difference. Strong meso- and submesoscale processes might have transported the coastal signals across the Red Sea. In addition, enhanced N_2O concentrations of up to 39 nmol L^{-1} were found at the seawater-brine pool interfaces which point to an N_2O production via nitrification and/or denitrification at low O_2 concentrations. Our results indicate that the Red Sea and the Gulf of Aqaba are unique natural laboratories for the study of N_2O production and consumption pathways under extreme conditions in one of the warmest and most saline region of the global oceans.

1. Introduction

Nitrous oxide (N_2O) is a trace gas which influences both the climate and the atmospheric chemistry of the Earth (IPCC et al., 2013; WMO, 2014): In the troposphere, it acts as a potent greenhouse gas whereas in the stratosphere it is involved in ozone depletion. The ocean (both open and coastal waters) is a major source of atmospheric N_2O (Anderson et al., 2010; IPCC et al., 2013). Microbial nitrification (i.e., oxidation of ammonia to nitrate) and denitrification (i.e., reduction of nitrate to

dinitrogen) are the main production and consumption pathways of N_2O in the ocean (Bakker et al., 2014; Bange, 2008; Freing et al., 2012). Nitrification occurs typically only under oxic/suboxic conditions, whereas denitrification occurs under suboxic/anoxic conditions (Devol, 2008; Ward, 2008). The amount of N_2O produced during nitrification depends on the concentration of dissolved oxygen (O_2). A (positive) linear relationship between excess N_2O (ΔN_2O) and apparent O_2 utilization (AOU) is found in large parts of the oxic ocean, see, e.g. Bange et al. (2010). This, in turn, implies that N_2O production via nitrification

is indirectly coupled to O_2-driven remineralisation of organic material in the oxic water column (Nevison et al., 2003; Yoshinari, 1976). Extreme N_2O accumulation of up to 55–80 nmol L^{-1} - resulting from denitrification and/or nitrification - has been found at the oxic/anoxic boundaries in the water columns of the Arabian Sea and the eastern tropical South Pacific Ocean (ETSP) (Bange et al., 2001; Kock et al., 2016).

The Red Sea is one of the warmest and most saline regions of the global ocean (Carvalho et al., 2019) and, therefore, may provide insights into future N_2O production/consumption pathways and nitrogen cycling in tropical oceans affected by the ongoing ocean warming. Here we present the first measurements of the N_2O water column distribution in the central Red Sea which is permanently stratified, and in the northern Gulf of Aqaba, which is characterized by seasonal turnover with deep winter mixing. Besides, we present the first measurements of N_2O in Red Sea brine pools. The overarching aims of our study were (i) to decipher the distribution of N_2O in the two basins, and (ii) to identify the main processes affecting the N_2O distribution.

2. Study sites and sampling campaigns

An overview about the sampling stations is given in Table 1.

2.1. Gulf of Aqaba

The Gulf of Aqaba is an extension of the northern Red Sea, separating the Sinai and Arabian Deserts. It is a deep basin with a maximum depth of about 1850 m, approximately 160–180 km in length, and 15–29 km wide (Rasul et al., 2015). It is separated from the northern Red Sea by a shallow sill (175 m) at the Straits of Tiran. The Gulf of Aqaba has a thermohaline circulation with a continuous inflow of oligotrophic surface waters from the Red Sea and an outflow of more dense, deep waters (Biton and Gildor, 2011). The seasonal setting of its water column is characterized by deep convective mixing during boreal winter (December to February) and a pronounced stratification during boreal summer (May to October) (Biton and Gildor, 2011; Wolf-Vecht et al., 1992). The waters of the Gulf of Aqaba are oxygenated and oligotrophic throughout the year (Manasrah et al., 2006; Wickham et al., 2015).

Water sampling for N_2O took place at the time-series site 'Station A' located in the northern Gulf of Aqaba (Fig. 1) during three sampling campaigns with the R/V *Queen of Sheba* in summer (June and September 2003) and winter (February 2004).

2.2. Central Red Sea

The Red Sea extends from 30°N to 12.5°N and lies between 32°E and 44°E. It has an average width of 220 km, and its maximum water depth is about 2860 m (Rasul et al., 2015). The only significant connection between the Red Sea and the global oceans is the Strait of Bab-al-Mandab, a shallow and narrow channel with a sill depth of about 137 m located at the southern end of the basin, which connects the Red Sea to the Gulf of Aden and the Arabian Sea/Indian Ocean. Due to its limited connection with the open ocean and the excess of evaporation over precipitation and river runoff, the Red Sea is one of the most saline basins in the world's oceans with water column salinities ranging from 35 to 43 (Sofianos and Johns, 2015; Sofianos and Johns, 2007). The Red Sea is characterized by a strong thermohaline and monsoon-driven circulation, shelf and open ocean water mass formation and a strong overturning circulation (Sofianos and Johns, 2015). The large-scale surface circulation pattern is governed by mesoscale eddy structures (Raitsos et al., 2017; Zarokanellos et al., 2017; Zhan et al., 2014; Kürten et al., 2019). Mesoscale structures are highly energetic and exhibit substantial temporal and spatial variability. They are known to play a major role in other semi-enclosed basins, such as the Black Sea (e.g., Kubryakov and Stanichny, 2015), the Caribbean Sea (e.g., Carton and Chao, 1999), and the Gulf of Mexico (e.g., Le Hénaff et al., 2012), including, for example, by the transport of coastal water into offshore regions. In the Red Sea, only limited information is available about the occurrence and characteristics of meso- or submesoscale activity. However, based on the relatively coarse altimetry data the highest number of eddies is found in the central Red Sea between 18°N and 24°N with radii ranging from 50 to 135 km and a lifetime of about six weeks (Zhan et al., 2014).

Table 1
Overview of sampling stations.

Station or Deep	Lat./Long. °N/°E	Sampling date	Bottom depth, m	Max sampling depth[a], m
Gulf of Aqaba				
Station A	29.47/34.93	June, Sept 2003; Feb 2004	750	740
Central and southern Red Sea				
NC1-1	23.67/37.11	Oct 2014	895	60
NC1-2	23.04/37.58	Oct 2014	1095	82
NC1-3	22.70/37.82	Oct 2014	965	923
NC1-4	22.35/38.13	Oct 2014	882	781
NC1-5	21.78/38.11	Oct 2014	1279	1259
NC1-6	21.39/38.07	Oct 2014	2000	1900
NC1-7	20.88/38.45	Oct 2014	945	942
NC1-8	20.55/38.62	Oct 2014	816	800
NC4-1	23.99/36.98	Jan 2016	890	880
NC4-2	21.76/38.13	Jan 2016	1362	1093
NC4-3	19.56/38.92	Jan 2016	1654	200
NC5-1	16.61/41.13	Aug 2016	1860	1860
NC5-2	19.61/38.72	Aug 2016	2827	2730
NC5-3	21.34/38.08	Aug 2016	2159	1500
Red Sea deeps				
Conrad[b]	27.06/34.73	Jan 2005	1505	1475–1500
Oceanographer[b]	26.28/35.01	Jan 2005	1560	1420–1555
Nereus[b]	23.19/37.25	Jan 2005	2460	2392
Thetis[b]	22.65/37.58	Jan 2005	1970	1965
Atlantis II (= NC5-3)	21.34/38.08	Aug 2016	2159	1990
Port Sudan (= NC5-2)	19.61/38.72	Aug 2016	2827	2771–2785

[a] For the Red Sea deeps the sampling depth (range) is given.
[b] Sampled during cruise RS05.
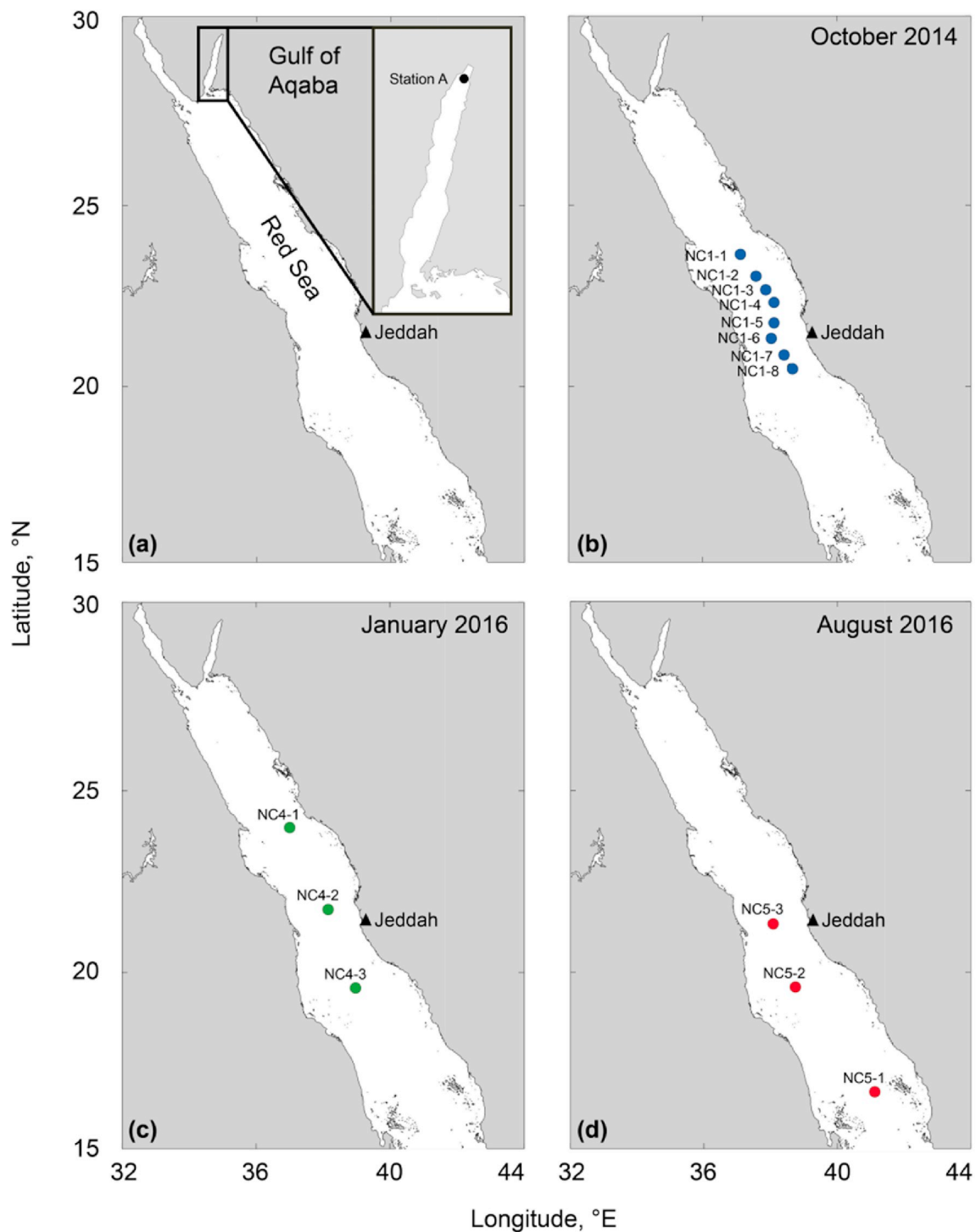
Fig. 1. Locations of the N$_2$O sampling stations (a) in the Gulf of Aqaba (June and September 2003, February 2004) and in the Red Sea during (b) October 2014 (cruise NC1), (c) January 2016 (cruise NC4) and (d) August 2016 (cruise NC5).

The Red Sea Deep Water (RSDW) fills the basin below approximately 150–250 m (Sofianos and Johns, 2015). These deep waters of the Red Sea are renewed through the sinking of dense waters originating in the northern Gulfs of Suez and Aqaba (Jean-Baptiste et al., 2004). The significant heat flux results in strong stratification throughout most of the basin and contributes to its overall and persistent oligotrophy (Naqvi et al., 1986; Qurban et al., 2017; Wafar et al., 2016). Although anthropogenic point sources of nutrients can affect shelf waters, nutrients become rapidly diluted and depleted within a few km offshore (Pena-Garcia et al., 2014). The central Red Sea

(20–25°N) is one of the most oligotrophic areas of the Red Sea and is located between the less productive northern (25–28°N) and the more productive southern (14–20°N) Red Sea (Raitsos et al., 2013). In contrast to the Gulf of Aqaba, the Red Sea has a pronounced oxygen minimum zone (OMZ) in the intermediate layers with minimum O$_2$ concentrations of about 10 µmol L^{-1} (Sofianos and Johns, 2007). The marked depletion of O$_2$ was explained by organic matter remineralisation in connection with a comparably long residence time of the RSDW which was estimated to range from 26 to 60 years (Jean-Baptiste et al., 2004).

Within the framework of the 'Nutrient Cycling in the Red Sea (NC)' project three cruises with R/V *Thuwal* were conducted from 24° to 19.6°N along the rift axis of the central Red Sea in fall (NC1: 20–28 October 2014), winter (NC4: 20–24 January 2016) and summer (NC5: 16–30 August 2016) (Fig. 1). During NC5, we collected additional samples at one station in the southern Red Sea at 16.5°N.

2.3. Brine-filled Red Sea deeps

Salty and slightly acidic (pH ~ 5–7) brine is covering the seafloor within depressions along the Red Sea rift axis (Schmidt et al., 2015). Brine pools are mainly formed by seawater which interacted with Miocene evaporite deposits from the underlying sediments. The highly saline and dense brine pools are separated from the RSDW by sharp interfaces where the exchange of heat and salt is controlled by diffusion (Anschutz et al., 1999; Swift et al., 2012). The brine layers are significantly depleted in O_2 and are anoxic in the deepest layer. In some cases, dissolved hydrogen sulphide (H_2S) has been detected (e.g., in the Kebrit and Oceanographer Deep) (Hartmann et al., 1998; Schmidt et al., 2015).

Samples from brine pools of the Conrad, Oceanographer and Nereus Deep as well as from a non-brine filled Thetis Deep were taken during the cruise RS05 with R/V *Urania* in January 2005 (Bonatti et al., 2005) (Fig. 2). Additionally, brine pools of the Port Sudan and Atlantis II Deeps were sampled during the cruise NC5 (see Section 2.2).

3. Data and methods

3.1. Nitrous oxide

The concentration of dissolved N_2O, $[N_2O]$, was determined by applying the static headspace equilibration method in combination
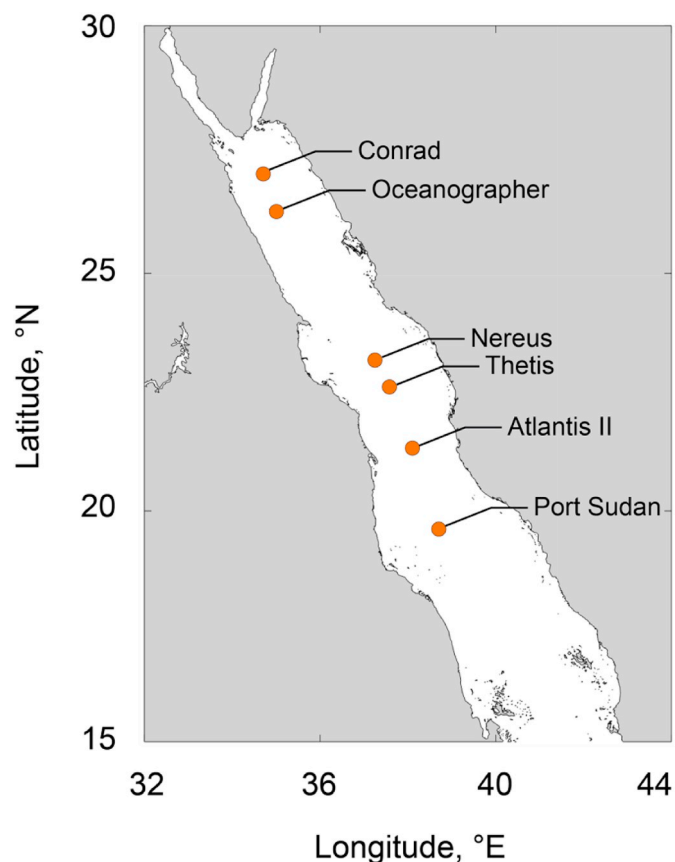
Fig. 2. Location of the Red Sea deeps sampled for N_2O.

with gas chromatographic separation followed by the detection of N_2O with an electron capture detector:

$$[N_2O] = x'PV_{hs}/(RTV_{wp}) + x'\beta P \tag{1}$$

where x' is the dry mole fraction of N_2O in the equilibrated headspace, P is the ambient pressure (set to 1 atm), V_{hs} and V_{wp} are the volumes of the headspace and the water phase, respectively. R stands for the gas constant ($8.2057\ 10^{-5}\ m^3\ atm\ K^{-1}\ mol^{-1}$), T is the temperature during equilibration and β is the solubility of N_2O. β was computed as a function of T and salinity (Weiss and Price, 1980).

Seawater samples for N_2O measurements from Station A in the northern Gulf of Aqaba were sampled in triplicates with 20 mL vials from Niskin bottles and immediately poisoned by adding 500 µL of 2 mM aqueous mercury chloride ($HgCl_2$) solution for later analysis at the chemical oceanography research unit of GEOMAR Helmholtz Centre for Ocean Research Kiel, Germany. Details of the analytical method are given in Walter et al. (2006a). The overall mean error of the N_2O measurements was ± 2% (calculated as the average of the estimated standard deviations of the triplicate measurements (David, 1951)).

During the NC cruises to the central Red Sea water samples for measurements of dissolved N_2O were tapped directly from Niskin bottles of the CTD/Rosette into 100 mL (NC1, NC4) and 20 mL (NC5) glass bottles. Immediately after collection, samples were preserved by adding saturated aqueous $HgCl_2$ solution. Triplicate N_2O samples were taken during cruise NC5, whereas, single N_2O samples were taken during cruises NC1 and NC4. A detailed description of the sample treatment, the analytical setup used for the measurements and computation procedures used to obtain N_2O concentrations can be found in Kock et al. (2016) and Pelz (2017), and references therein. The overall mean error of the N_2O measurements during cruise NC5 was ± 9% (calculated as the average of the estimated standard deviations of the triplicate measurements (David, 1951)).

Brine samples were taken from Niskin bottles immediately after the CTD/Rosette was on deck. Water was tapped into 120 mL glass bottles and preserved by adding saturated aqueous $HgCl_2$ solution. Samples were analysed with a gas chromatographic system, as described in Walter et al. (2006a). No replicates were taken. Because the samples were analysed for dissolved inorganic carbon first, a headspace had been added to the samples before they arrived at GEOMAR's laboratory for subsequent N_2O analysis. Therefore, we needed to correct the final N_2O concentrations of the RS05 samples by adjusting them to the mean deep water N_2O concentration from the NC cruises. A correction factor of 0.4 was estimated as $[N_2O]_{dwNC}$: $[N_2O]_{dwRS05}$, where $[N_2O]_{dwRS05}$ is the mean of the RS05 deep water N_2O concentrations (from 200 m to brine pool/deep water interface) and $[N_2O]_{dwNC}$ is the mean NC deep water concentrations (i.e., from > 200 m).

N_2O saturations (N_2O_{sat} in %) and ΔN_2O were calculated as $N_2O_{sat} = 100*[N_2O]/[N_2O]_{eq}$ and $\Delta N_2O = [N_2O] - [N_2O]_{eq}$, respectively. $[N_2O]$ stands for the measured in-situ concentration of N_2O (see equation (1) above) and $[N_2O]_{eq}$ stands for the equilibrium concentration of N_2O computed with the equation given in Weiss and Price (1980) based on the atmospheric N_2O dry mole fraction as well as the measured water temperature and salinity at the time of the measurement campaigns. The total ambient atmospheric pressure was set to 1 atm. Atmospheric N_2O dry mole fractions were taken from the atmospheric time series measurements at the monitoring station Mace Head (Ireland) which is part of the Advanced Global Atmosphere Gases Experiment (AGAGE) project (data are available from https://agage.mit.edu/). For the computation of $[N_2O]_{eq}$, we did not account for the ages of the sampled deep water masses (Freing et al., 2012) because they are not known. Therefore, $[N_2O]_{eq}$ for deep waters is biased towards higher values and results in lower N_2O_{sat}. With the assumption of a mean residence time of the RSDW (taken as a rough proxy of the deep water mass age) of about 26–60 years (Jean-Baptiste et al., 2004) -
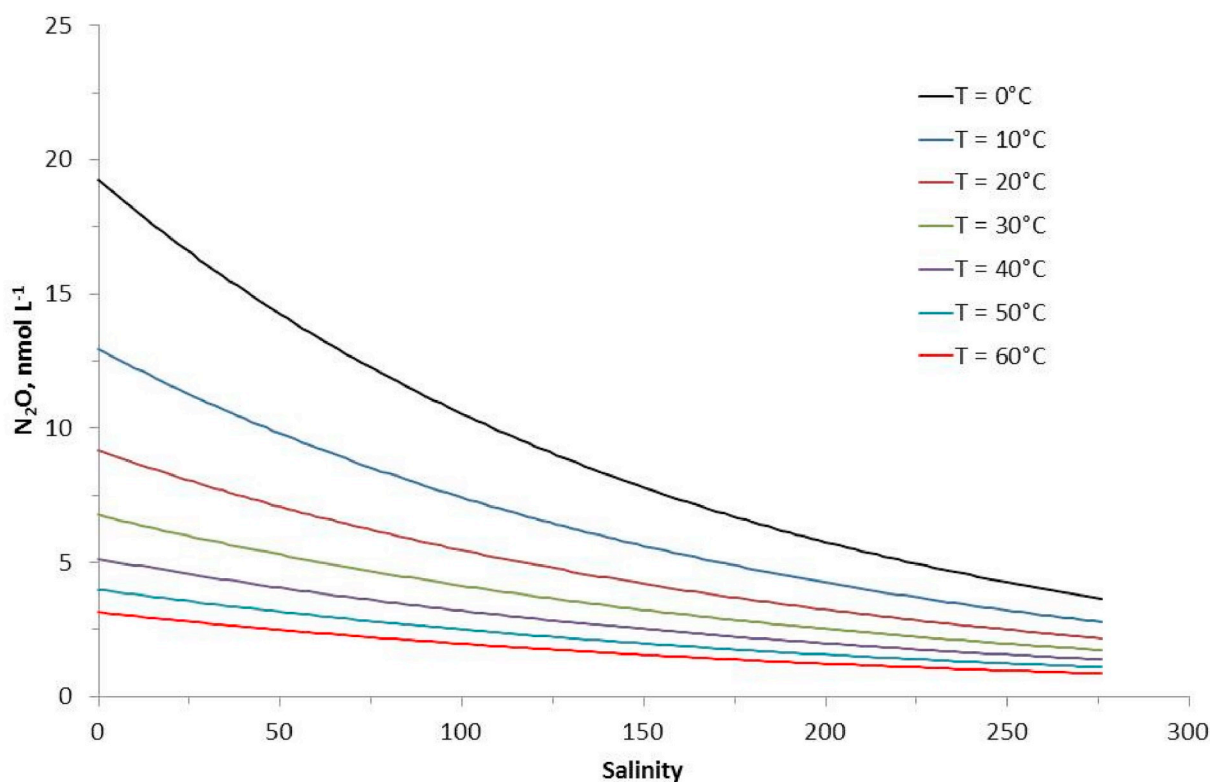
Fig. 3. Dissolved N_2O concentrations as a function of salinity and temperature (Weiss and Price, 1980). Atmospheric dry mole fraction of N_2O was set to 328 ppb and total atmospheric pressure was set to 1 atm.

which would be associated with mean atmospheric N_2O mole fractions of 310 ppb (see GAGE data set at http://agage.eas.gatech.edu/data_archive/gage/monthly/) and 290 ppb (Ishijima et al., 2007) in 1990 and 1956, respectively - we estimate that the 'true' (i.e., water mass age corrected) $[N_2O]_{eq}$ for deep waters may be lower by about 6–12%.

The solubility equation of Weiss and Price (1980) has been established for salinities in the range from 0 to 40. However, the majority of the water column measurements presented here had salinities > 40, and the salinity of brines were up to 275. Fig. 3 shows the N_2O concentrations as a function of salinity for temperatures from 0 to 60 °C computed with the equation of Weiss and Price (1980). When applying a linear extrapolation of the Weiss and Price (1980)'s values to salinities of 40–50, the resulting concentration difference is negligible. However, concentration differences become unrealistically large when applying a linear extrapolation to very high salinities. Therefore, we decided to use the equation by Weiss and Price (1980) for salinities > 40 even though the solubility function of N_2O is not known for the high salinity range.

3.2. CTD, nutrients and oxygen measurements

Vertical profiles of conductivity, temperature, depth (CTD) were measured with commonly used standard CTD systems. Seawater samples for the determination of dissolved nitrate (NO_3^-), nitrite (NO_2^-) and phosphate (PO_4^{3-}) were taken from Niskin bottles and measured with a continuous flow analyser according to standard spectrophotometric methods (Grasshoff et al., 1999) immediately after the sampling trips to Station A at the Interuniversity Institute Laboratory in Eilat, Isreal. Nutrient samples from the NC cruises were frozen to −20 °C on-board and stored at −80 °C in the laboratory until analysis at King Abdullah University of Science and Technology (KAUST), Saudia Arabia, by using a continuous flow analyser (AA3 HR, SEAL, USA) following the designated methods. Nutrient data from the NC1 cruise are presented in Kürten et al. (2019). Nutrient measurements from the RS05 cruise are not available.

Dissolved O_2 concentrations in discrete seawater samples from Niskin bottles were measured following the Winkler titration method (Grasshoff et al., 1999; Winkler, 1888) in the laboratory shortly after collection at Station A. O_2 concentrations from the NC cruises were derived from O_2 sensors at the CTD/Rosette which have been calibrated by the manufacturer. O_2 concentrations were not measured during RS05. AOU was calculated as $AOU = [O_2]_{eq} - [O_2]$, where $[O_2]$ stands for the measured in-situ concentration of O_2 and $[O_2]_{eq}$ stands for the equilibrium concentration of O_2 computed with the equation given in Weiss (1970).

3.3. Satellite data

We used the daily, 4 km resolution, level-3 remotely-sensed sea surface temperature (SST) (unit: °C) and surface chlorophyll (Chl) (unit: mg m^{-3}) measurements from the Moderate Resolution Imaging Spectroradiometer (MODIS-Aqua) produced by the NASA Ocean Biology Processing Group, which are freely available from the NASA website (http://oceancolor.gsfc.nasa.gov/). The purpose of using high resolution (4 km) SST and Chl maps is to use the signals as a tracer of spatial variations, to identify meso- or submesoscale structures during the field campaigns. To fulfill that task, satellite-based altimetry data is often used in other parts of the globe, but due to its coarse resolution (0.25°) and the omnipresent vicinity of nearby land in the Red Sea, altimetry data is not well suited to find mesoscale or even submesoscale structures in the Red Sea.

4. Results and discussion

4.1. Northern Gulf of Aqaba

The N_2O surface concentrations (Fig. 4a) and saturations (Fig. 4b) in the northern Gulf of Aqaba ranged from 6 to 8 nmol L^{-1} and 97–111%, respectively, and were close to the equilibrium with the overlying
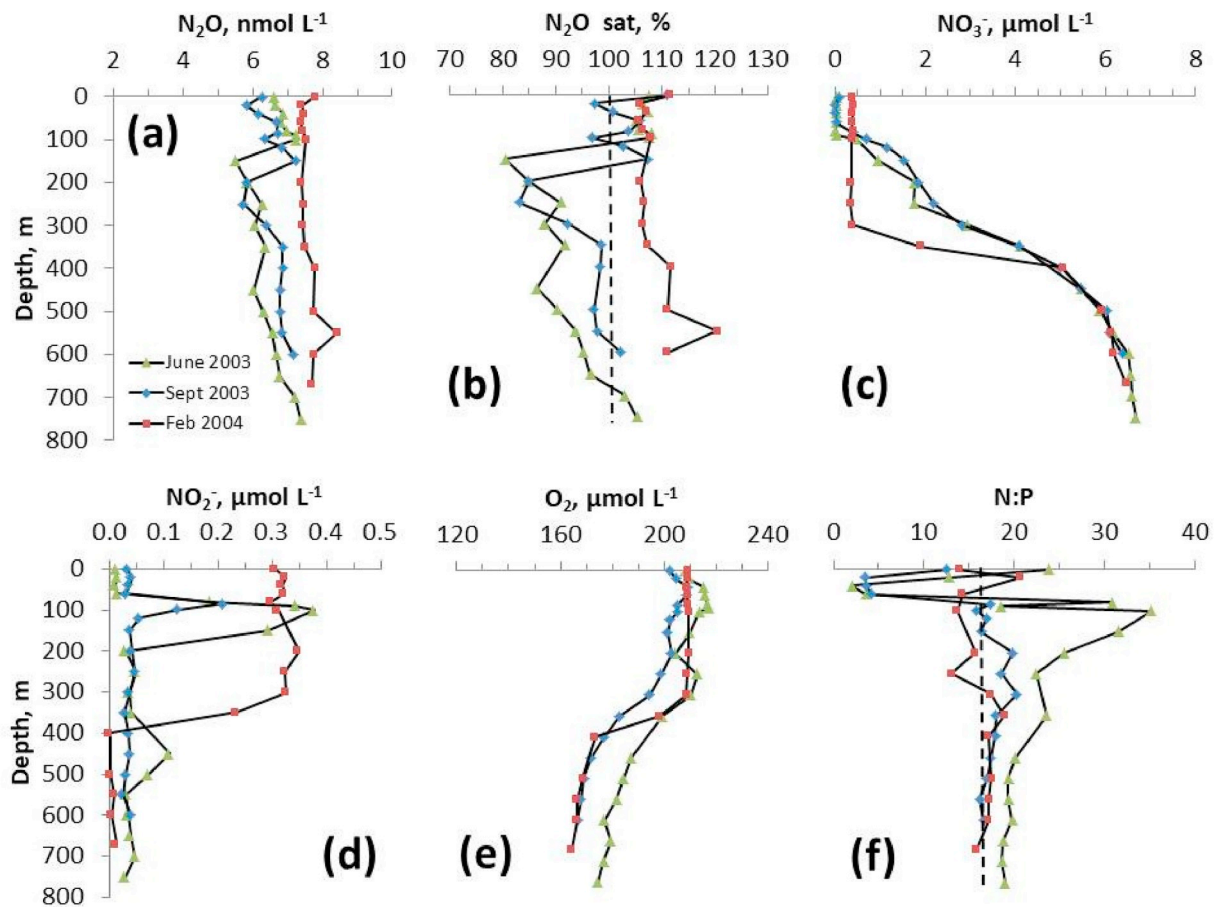
Fig. 4. Depth profiles of (a) N_2O, (b) N_2O saturations, (c) NO_3^-, (d) NO_2^-, (e) O_2 and (f) N:P ratio at Station A in the northern Gulf of Aqaba. The dashed lines indicate 100% saturation (= equilibrium saturation) and the N:P ratio of 16 in (b) and (f), respectively. Green triangles depict data from June 2003, blue squares depict data from September 2003, and red squares depict data from February 2004. Please note that the N_2O data are averages of triplicate measurements; however, errors bars are not shown to enhance clarity of the plots. (For interpretation of the references to colour in this figure legend, the reader is referred to the Web version of this article.)

atmosphere. A significant N_2O consumption in the surface layer by denitrifiers associated with *Trichodesmium* colonies, as recently suggested to take place in the Gulf of Aqaba (Coates and Wyman, 2017), was not observed. The depth distributions of N_2O during summer (June and September 2003) were similar. They showed a slight increase in concentrations from the ocean surface down to 100–150 m which was followed by a drop in concentrations and again a slight increase in the deep layers towards the bottom (Fig. 4a). The decrease in N_2O concentration was (i) associated with increasing NO_3^- concentration below the NO_3^--depleted surface layer (0–100 m) (Fig. 4c) and (ii) located just below the nitrite maximum in June and September 2003 (Fig. 4d). The slight increase of N_2O concentrations in the deep water (> 200 m) correlated with a decline in O_2 concentrations towards the bottom (Fig. 4e). In contrast, the N_2O profile from the winter (February 2004) was comparably uniform throughout the water column. N_2O concentrations during summer (June and September 2003) were lower compared to the N_2O concentrations in winter (February 2004). In contrast to the N_2O surface saturations, waters below 150–200 m were significantly undersaturated in summer (June and September). N_2O saturations in winter (February) were supersaturated throughout the water column (Fig. 4b).

The obvious temporal variability of the N_2O concentrations was most probably driven by (i) the deep mixing of the water column during winter which results in a uniform N_2O depth distribution with concentrations slightly above the atmospheric equilibrium concentration and (ii) the marked stratification during summer which led to the pronounced decrease of the N_2O concentrations in the deep water

below the surface layer. During the course of our study the water column was well-oxygenated with O_2 concentrations > 160 μmol L^{-1} which, in turn, favours nitrification in the water column at Station A. This is in line with the results by Mackey et al. (2011) and Meeder et al. (2012) who stated that nitrification is present at Station A and responsible for the build-up of a nitrite maximum in summer (see Fig. 4d). However, we found a positive linear correlation between ΔN_2O and AOU (Fig. 5) only for February and in deep waters with AOU > 25 μmol (O_2 concentrations < 190 μmol L^{-1}). This implies that N_2O was resulting from nitrification in the entire water column in winter whereas in summer N_2O seemed to be produced by nitrification only in the deep waters. (Please note that O_2 concentrations < 190 μmol L^{-1} were only found below 300 m (see Fig. 4e)).

The failure to detect a linear ΔN_2O/AOU relationship in the upper water column (O_2 concentrations > 190 μmol L^{-1}) in summer is caused by the N_2O undersaturation measured below the surface layer. N_2O undersaturations in well-oxygenated waters are unexpected because nitrification does not involve an N_2O consumption step. N_2O consumption via denitrification can be excluded in the well-oxygenated subsurface waters of Station A. An alternative explanation for the drop of the N_2O concentrations during summer might be consumption of N_2O through biological nitrogen (N_2) fixation (Farías et al., 2013). Indeed, Rahav et al. (2013) detected significant N_2 fixation in the aphotic deep layer at Station A. This is in line with the observation that the N:P ratios (= ($[NO_3^-]$ + $[NO_2^-]$)/$[PO_4^{3-}]$) during summer showed a pronounced increase from < 4 to 35 at 100 m and from 16 to 20 at 200 m in June 2003 and September 2003, respectively (Fig. 4f), which
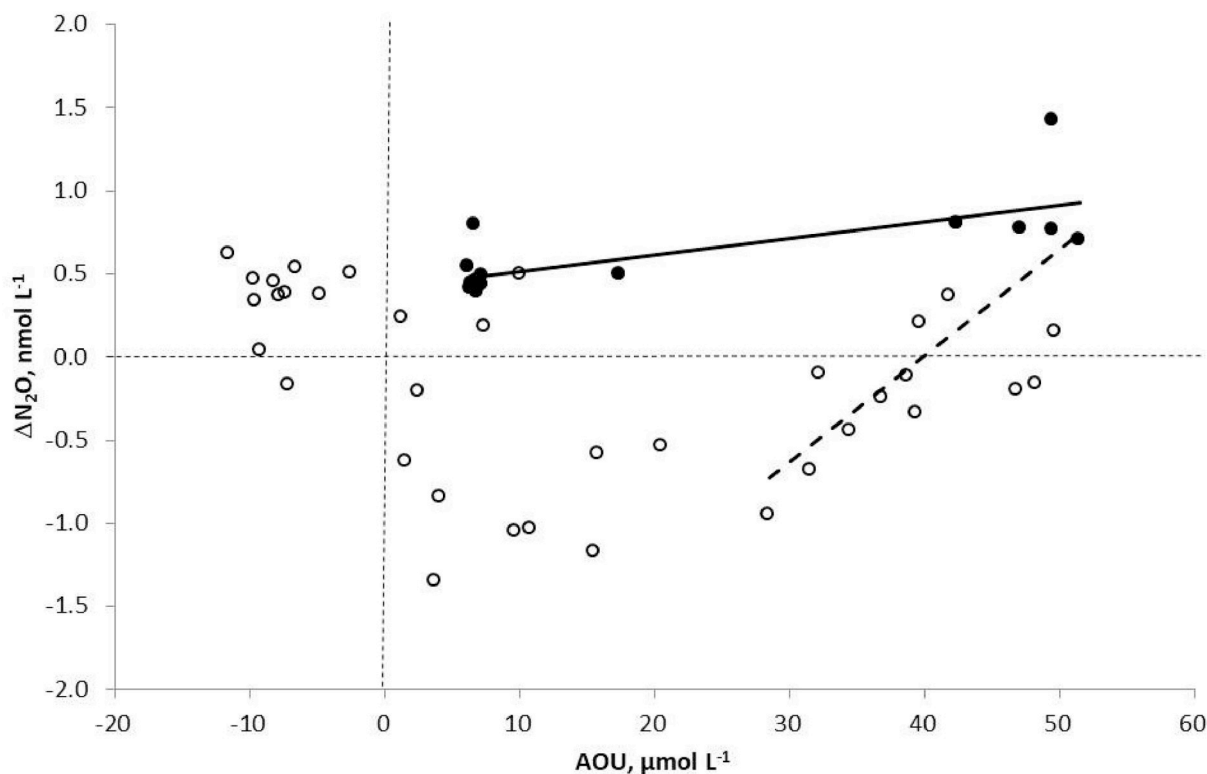
Fig. 5. ΔN_2O and AOU at Station A in the northern Gulf of Aqaba. The trend lines for data from February and for AOU > 25 μmol L^{-1} are indicated: the solid line is the trend line for the February data (filled circles; ΔN_2O = 0.064*AOU – 2.541; R^2 = 0.55, n = 15; significant at the 99% level) and the dashed line is the trend line for all data with AOU > 25 μmol L^{-1} (ΔN_2O = 0.009*AOU – 0.415; R^2 = 0.53, n = 17; significant at the 99% level).

implies that N_2 fixation took place. Moreover, it is intriguing to see that the increase of N:P to values > 16 is associated with the drop in the N_2O concentrations. These findings suggest that the N_2O production via nitrification is compensated by N_2O consumption via N_2 fixation during summer in the deep layer.

4.2. Central Red Sea

The N_2O concentration depth profiles showed a pronounced temporal variability with higher concentrations in October 2014 compared to January and August 2016 (Fig. 6). The variability of the N_2O concentrations throughout the water column in October 2014 and January 2016 was remarkably low and ranged from 7 to 9 nmol L^{-1} and 5–7 nmol L^{-1}, respectively. This is in contrast to the N_2O concentrations in August 2016, which ranged from 2 to 8 nmol L^{-1}. N_2O saturations in October 2014 were supersaturated and ranged from 155% at 10 m to 109% at 1900 m (Fig. 7). In January and August 2016, however, the water column was generally undersaturated with a minimum N_2O saturation of only 43% at 10 m in August 2016.

4.2.1. Surface layer

The range of N_2O surface saturations in October 2014 (135–155% at 10 m depth) are in reasonable agreement with the only other available N_2O measurements from the Red Sea: Weiss et al. (1992) measured N_2O surface saturations ranging from 97 to 133% along a North-to-South transect from the Gulf of Suez to the Gulf of Aden in December 1977/ January 1978. The very low N_2O concentrations in the surface layer in January and August 2016 (43–83% at 10 m) are unexpected because consumption of N_2O in surface layers is traditionally thought to be non-existing due to high O_2 concentrations which should preclude N_2O consumption via denitrification. However, this paradigm was recently challenged by findings of the abundance and activity of the *nosZ* gene (which encodes the N_2O reductase of the denitrification pathway) in

oxygenated surface waters (Coates and Wyman, 2017; Raes et al., 2016; Sun et al., 2017). Comparable to our results, N_2O depletion with undersaturations as low as 35% in the surface layer of the oligotrophic eastern subtropical South Pacific Ocean was also reported by Cornejo et al. (2015). Based on $^{15}N_2O$ uptake experiments, Cornejo et al. (2015) attributed this phenomenon to N_2O consumption via N_2 fixation in the oxygenated surface layer. The Red Sea is well-known for the occurrence of diazotrophs, see e.g. Böttger-Schnack and Schnack (1989) and Halim (1969). The assessment of the plankton communities during the NC cruises revealed the presence of *Trichodesmium* and other diazotrophs (diatom-diazotroph associations) in the euphotic zone (Kürten et al., 2019, and unpublished data). Fig. 8 shows a comparison of the mean N_2 fixation rates (Kürten et al., unpublished data) and the mean ΔN_2O, both integrated for the euphotic zone. The switch from N_2O production in October 2014 to N_2O consumption in January and August 2016 is not related to an enhancement of the N_2 fixation rates. N_2O production was dominating potential N_2O consumption by N_2 fixation in October 2014 (Fig. 8). Qurban et al. (2014) suggested that nitrification could be an important source of nitrogen for primary production in the Red Sea. This implies that nitrification could have been a potential source of N_2O in the euphotic zone in October 2014. In January and August 2016, however, the Red Sea was influenced by the strong El Niño-Southern Oscillation event (ENSO) in 2015/16 (Osman et al., 2018; Santoso et al., 2017). It was suggested that El Niño events enhance the overall productivity of the Red Sea (Raitsos et al., 2015). However, phytoplankton is outcompeting nitrifiers in terms of NH_4^+ uptake, see e.g. Ward (2008). To this end, we may speculate that an El Niño-triggered enhanced biological productivity may have led to a decrease of nitrification allowing N_2 fixers and/or *Trichodesmium* associated denitrifiers (Coates and Wyman, 2017) to overwhelm N_2O production with N_2O consumption.
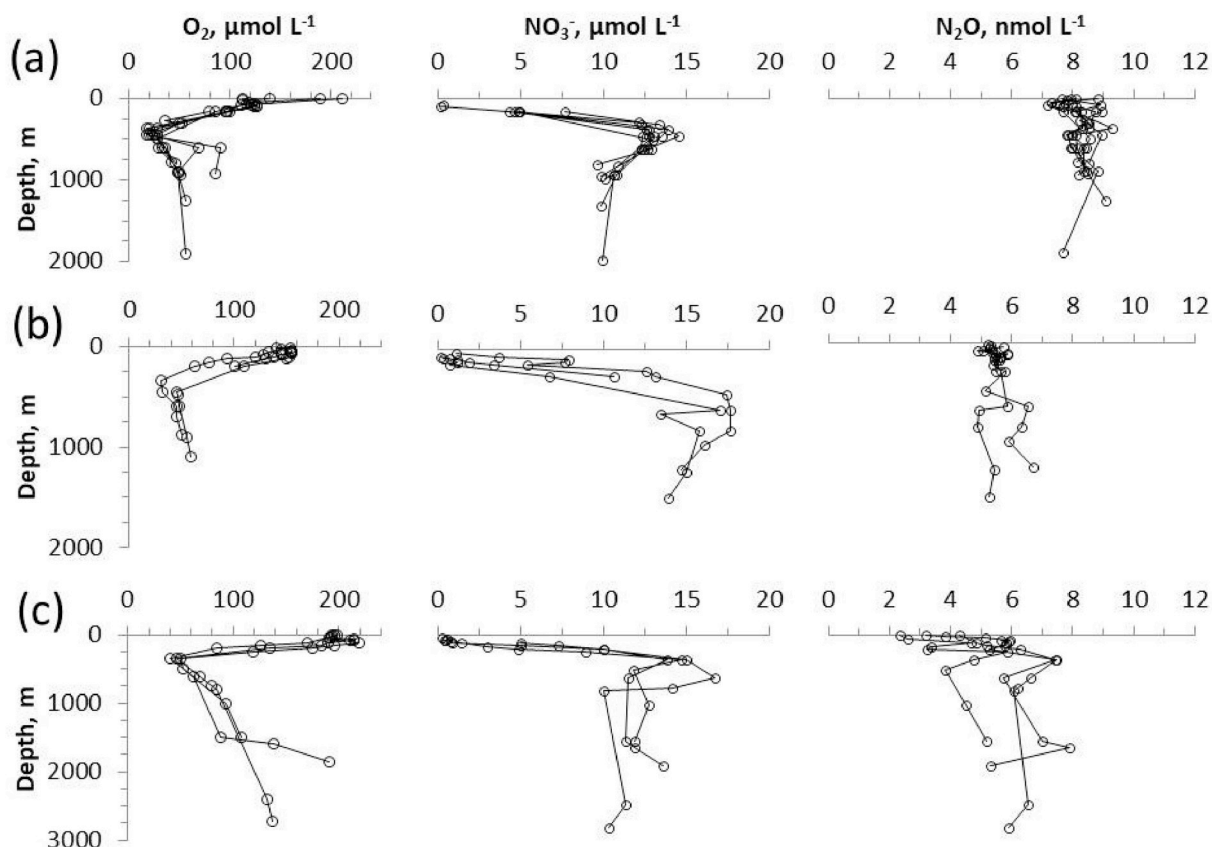
Fig. 6. Dissolved O_2, NO_3^- and N_2O concentrations in the central Red Sea: (a) October 2014, (b) January 2016, and (c) August 2016. Please note that the N_2O data from August 2016 are averages of triplicate measurements; however, errors bars are not shown to enhance clarity of the plot.
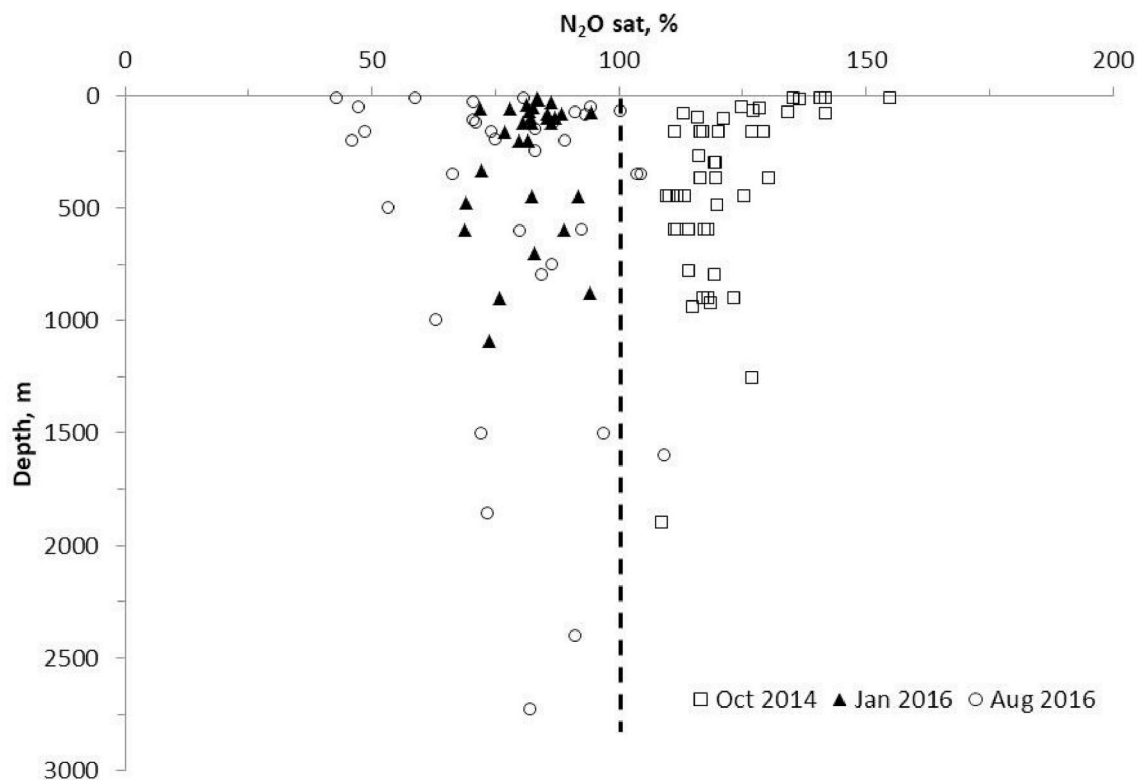
Fig. 7. N_2O saturations in the Red Sea in October 2014 (filled squares), January 2016 (filled triangles), and August 2016 (open circles). 100% N_2O equilibrium saturation is indicated by a dashed line.
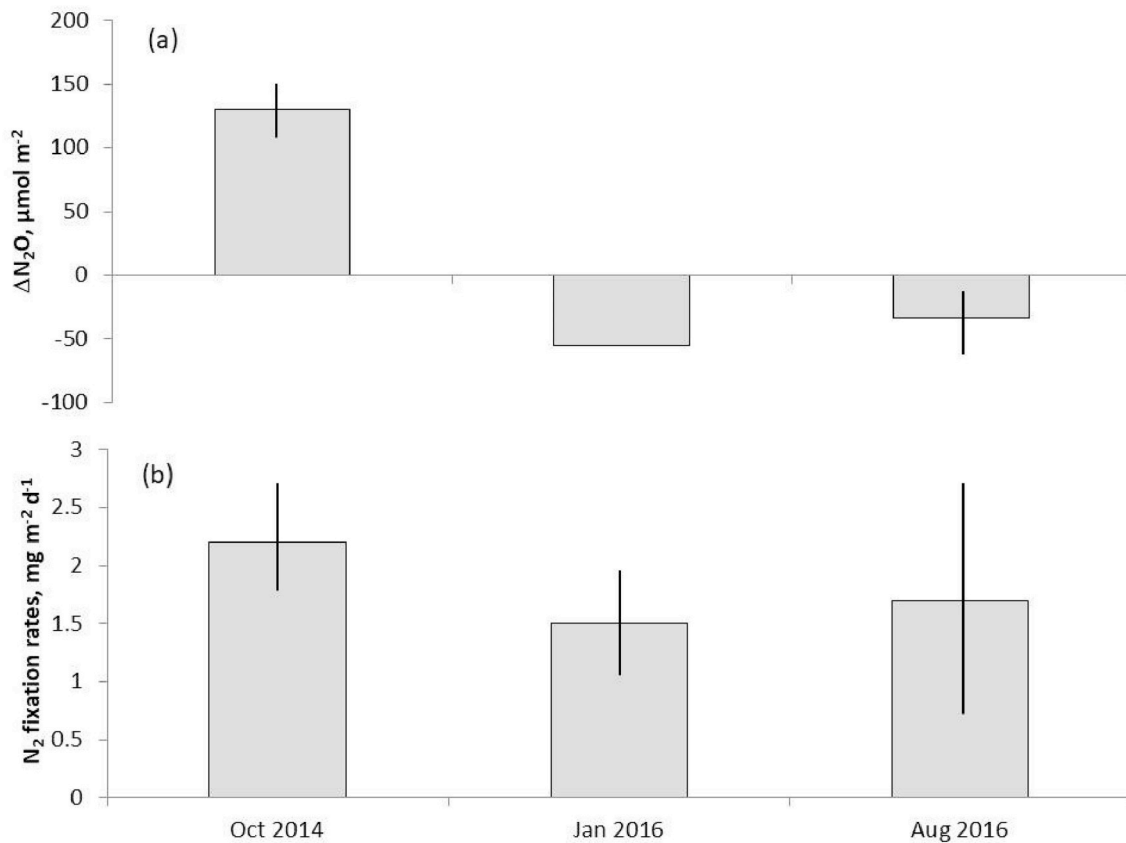
Fig. 8. (a) Mean ΔN_2O concentrations ($+/-$ standard deviation) integrated for the euphotic zone. (Please note that for January 2016 we have measurements only for the euphotic zone at one station.) (b) Mean N_2 fixation rates ($+/-$ standard deviation) integrated for the euphotic zone (Kürten et al., unpublished data).

4.2.2. Intermediate and deep waters

We observed a pronounced OMZ between 400 and 500 m water depth with a minimum O_2 concentration of $18\,\mu mol\,L^{-1}$ in October 2014 (Fig. 6). The characteristic positive linear correlation between ΔN_2O and AOU, which is a common feature found in many OMZ (Bange, 2008; Nevison et al., 2003), was only apparent when correlating the minimum AOU found at each station with the ΔN_2O at the same depth (Fig. 9). The resulting $\Delta N_2O/AOU$ ratio of $0.1\,*10^{-3}$ is comparable to $\Delta N_2O/AOU$ ratios from the adjacent western and central Arabian Sea ($0.03\,*10^{-3}$ - $0.3\,*10^{-3}$) (Bange et al., 2001) and the northern Gulf of Aqaba (Fig. 5).

The decrease in N_2O concentrations in the water column between October 2014 and January 2016 implies a significant N_2O loss. The depth distribution of N* (computed as N* = ([NO_3^-] + [NO_2^-]) − $16*[PO_4^{3-}]$) shows a minimum with values down to $-3\,\mu mol\,L^{-1}$ at depths of 400–500 m in October 2014 coinciding with the OMZ (Fig. 10). In January and August 2016, negative N* values did occur. However, a clear minimum was not visible. In January 2016, some N* values ranged up to $3\,\mu mol\,L^{-1}$ in water depths between 100 and 700 m. On the one hand, N* values < 0 point to a nitrogen loss via denitrification. On the other hand, N* values > 0 point to a nitrogen gain via N_2 fixation. Therefore, we may conclude that the supersaturation of N_2O in October 2014 was indeed resulting from the onset of denitrification at the low O_2 concentration of $18\,\mu mol\,L^{-1}$ in the OMZ and nitrification in the rest of the oxic water column. The N_2O undersaturations in January 2016 might have resulted from N_2O consumption via (aphotic) N_2 fixation comparable to the phenomenon seen in the northern Gulf of Aqaba (see above) as indicated by N* > 0 (Fig. 10). The N_2O undersaturations were still measurable in August 2016 although no indication of N_2 fixation (i.e., N* > 0) was apparent (Fig. 10). This suggests that in August 2016 N_2O consumption via N_2 fixation disappeared but N_2O production was too weak or even absent

to compensate for the N_2O loss. The N* values were < 0 in August 2016 (and in some depths in January as well) indicating a denitrification signal at O_2 concentrations of > $30\,\mu mol\,L^{-1}$. These comparably high O_2 concentrations are above the threshold for the onset of denitrification ($\sim 20\,\mu mol\,L^{-1}$) (Cornejo and Farías, 2012; Zamora et al., 2012). We suggest that the nitrogen inventory – as indicated by the N* values and N_2O concentrations – was also affected by remote (coastal) processes in combination with mesoscale and submesoscale circulation patterns (i.e., eddies or filaments). Snapshots of high-resolution satellite observations of SST and Chl during our field campaigns (Fig. 11) indicate a high meso- and submesoscale activity. These processes may help to explain the signals of coastal nitrogen processes such as low N* values and low N_2O concentrations in the more offshore study area (see here, in particular, the central and southern sampling stations during the field campaign in January 2016, Fig. 11b and e). Nitrogen loss resulting from denitrification has been observed in the coastal waters receiving nutrient-enriched sewage from the city of Jeddah (Orif et al., 2017; Pena-Garcia et al., 2014) located at $\sim 21.5°N$ at the east coast of the Red Sea. Furthermore recent results from a study of nitrogen cycling in seagrass meadows at the east coast of the central Red Sea Garcias-Bonet et al. (2018) showed a significant nitrogen loss due to sedimentary denitrification and anaerobic ammonia oxidation (anammox). Since mangroves are found along the entire Red Sea coast (Khalil, 2015), pristine mangrove may also contribute to N_2O consumption (Maher et al., 2016). To this end, we speculate that N_2O consumption in coastal regions (including lagoons, seagrass and mangrove ecosystems) results in N_2O undersaturated water which is transported due to meso- and submesoscale processes into the open Red Sea. Moreover, a deepening of the isopycnals attributable to anticyclonic eddies or the enhanced vertical velocities associated to submesoscale filaments or fronts may further contribute to the unusual N_2O distribution measured in the intermediate and deep layers of the central Red Sea.
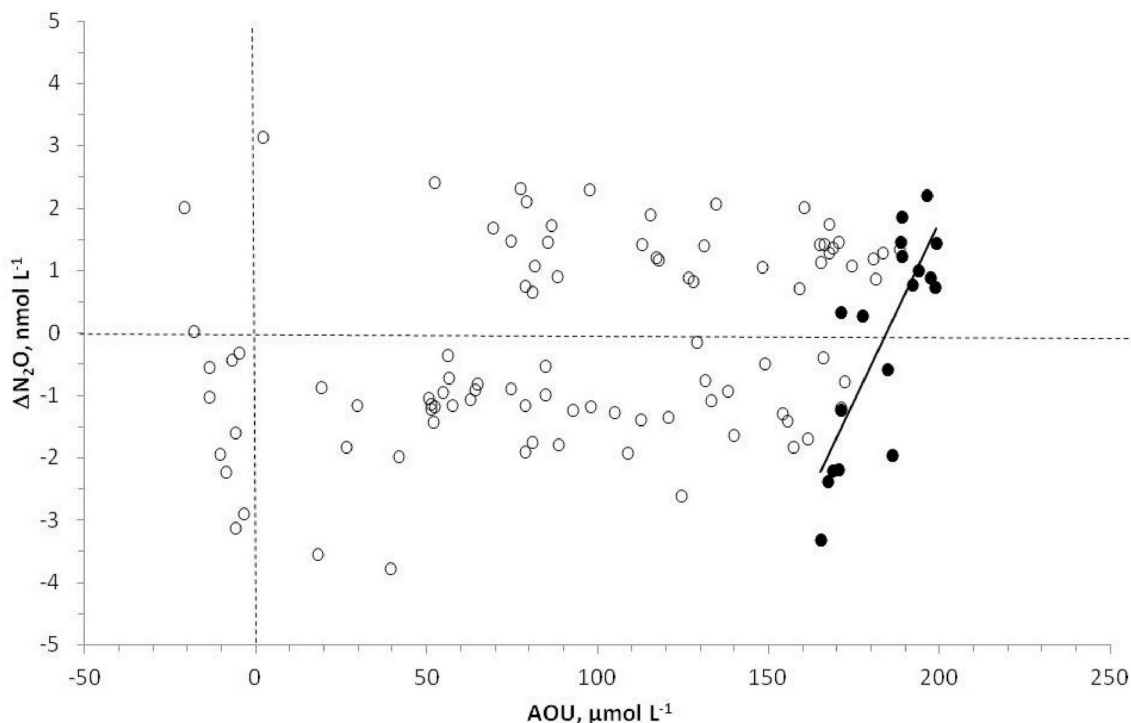
Fig. 9. ΔN_2O and AOU in the Red Sea. The trend line (filled circles; $\Delta N_2O = 0.116*AOU - 21.3$; $R^2 = 0.66$, n = 19; significant at the 99% level) is calculated for the minimum AOU at each station and its associated ΔN_2O measured at the same depth.

4.3. Red Sea deeps

The depth distributions of N_2O concentrations in the brine pools of the Oceanographer and Conrad Deeps are shown in Fig. 12. N_2O concentrations in the brine pool below the seawater-brine interface are uniform and concentrations $< 5\,nmol\,L^{-1}$ suggest a dominance of physical processes such as mixing and diffusion (e.g., Anschutz and Blanc (1996)) over potential production and consumption processes within the brine. A notable enhancement of N_2O with a maximum concentration of up to $39\,nmol\,L^{-1}$ at the seawater-brine interface was also observed for some of the brine pools and indicates N_2O production at the interface (Fig. 13). Since no dissolved O_2 and nutrient measurements are available from the RS05 cruise, we can only speculate about the processes leading to the accumulation of N_2O at the interface.
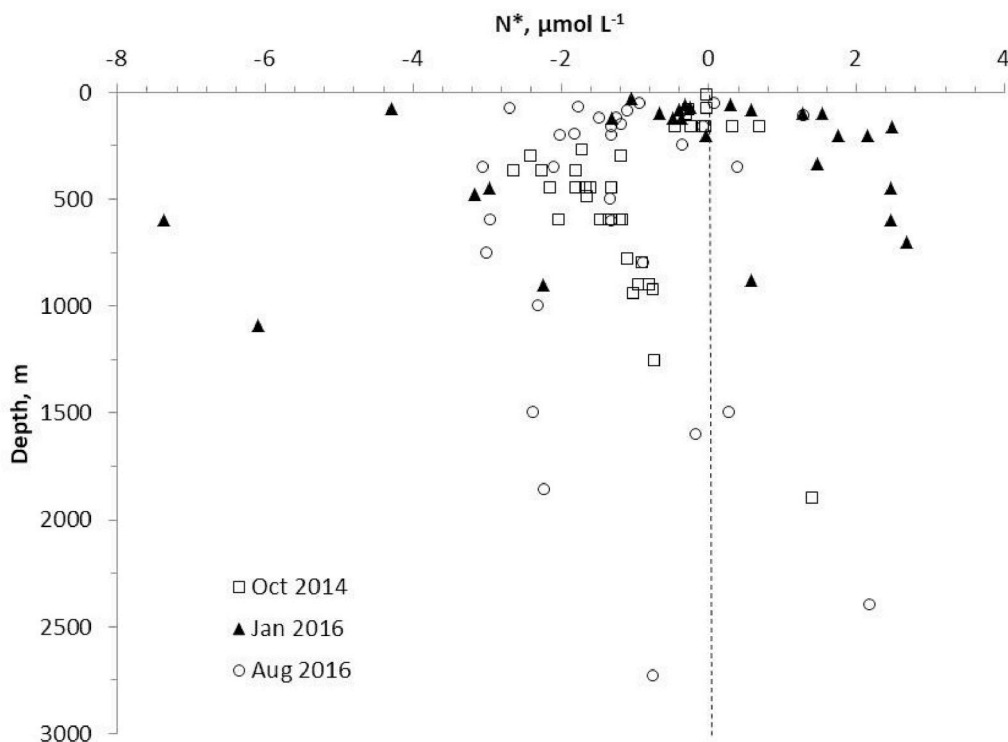
Fig. 10. N* in the Red Sea in October 2014 (open squares), January 2016 (filled triangles) and August 2016 (open circles). N* = 0 is indicated by a dashed line.
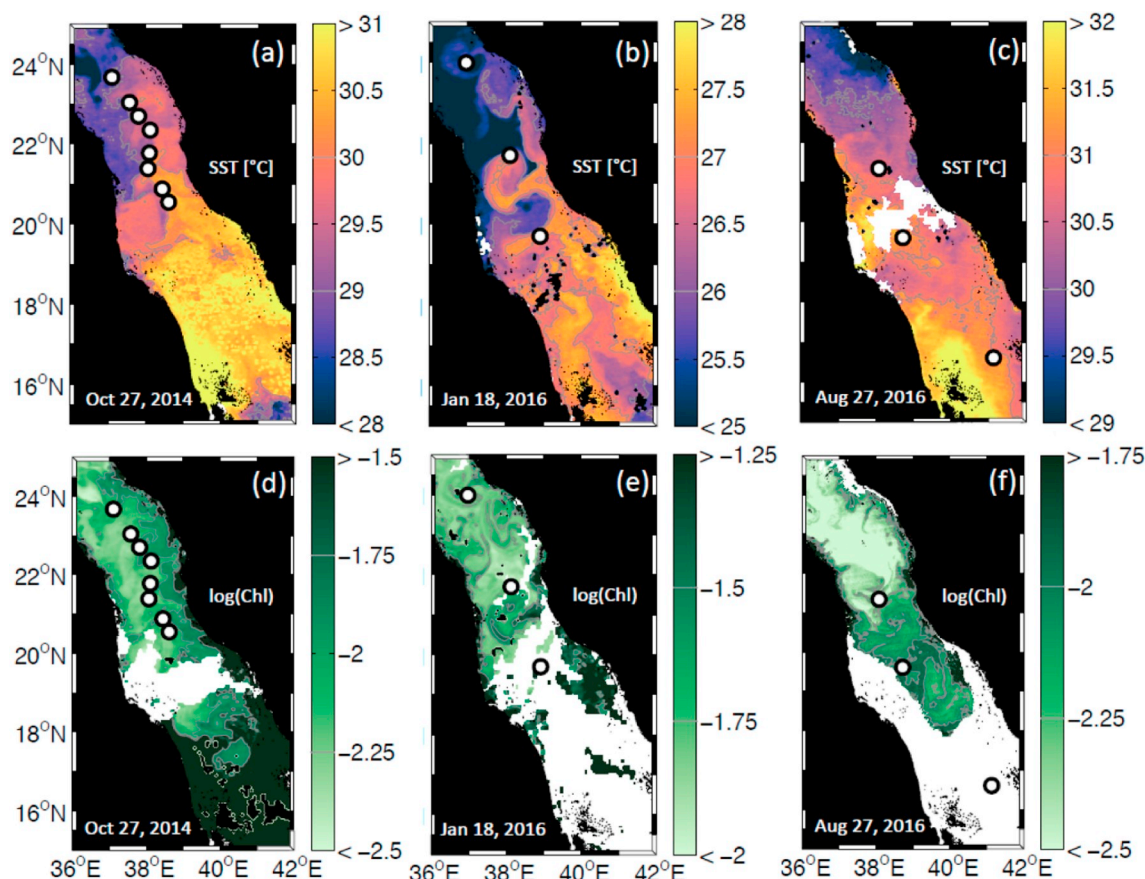
Fig. 11. Snapshots of remotely-sensed sea surface temperature (SST) and ocean colour observations (Chl) portraying mesoscale and submesoscale surface patterns in the central Red Sea on 27 October 2014 (a, d), 18 January 2016 (b, e), and 27 August 2016 (c, f). SST (°C) is shown in the upper panels (a)–(c) and Chl (mg m^{-3}, please note the logarithmic scale) is shown in the lower panels (d)–(f). The locations of the sampling stations are indicated by the white dots. White areas indicate no data.

We assume that the biogeochemical settings at the seawater-brine interfaces of the deeps sampled in our study are characterized by a steeply declining O_2 gradient associated with the extreme density gradient (Eder et al., 2002; Hartmann et al., 1998; Schmidt et al., 2003). These strong gradients can act as a 'trap' for organic and inorganic materials from the seawater above and increase the nutrient supply and potential for microbial growth (Antunes et al., 2011; Eder et al., 2001). Anaerobic organic matter degradation may take place at the seawater-brine interface (Eder et al., 2001). Moreover, ammonia oxidizing (i.e., nitrifying) archaea were found at the seawater/brine pool interface at various Red Sea deeps and point to potential nitrification at these sites (Cao et al., 2015; Ngugi et al., 2015). The results of a recently published culture study revealed that denitrifying halophilic archaea can produce significant amounts of N_2O (Torregrosa-Crespo et al., 2019). Similar to observations at the oxic/anoxic boundaries in the Arabian Sea (Bange et al., 2001), the eastern tropical South Pacific (Ji et al., 2015; Kock et al., 2016), and the Baltic and Black Seas (Walter et al., 2006b; Westley et al., 2006), the present study suggests that N_2O production at the seawater-brine interface in the Red Sea is attributable to N_2O production via nitrification and/or denitrification at low O_2 concentrations.

5. Summary

The water column distribution of N_2O in the northern Gulf of Aqaba and the central Red Sea showed a pronounced variability driven by a complex interplay of biological and physical processes. The temporal variability of N_2O at Station A in the northern Gulf of Aqaba was attributed to the combined effects of (i) production via nitrification, (ii)

consumption via N_2 fixation below the surface layer during summer and (iii) deep mixing during winter. N_2O in the water column of the central Red Sea was supersaturated in October 2014 and mainly resulted from its production via nitrification, whereas, low N_2O concentrations in the surface and deep layers in January and August 2016 indicated a significant loss of N_2O since October 2014. We speculate that the potential N_2O loss in the central Red Sea was resulting from N_2 fixation. Additionally, we surmise that signals from remote N_2O loss processes such as denitrification in coastal areas could have been transported to the open Red Sea by meso- and submesoscale processes (e.g., eddy core transport or eddy stirring).

Moreover, we present the first N_2O concentration data from various brine pools of the Red Sea. At the seawater-brine interfaces, enhanced N_2O concentrations point to an N_2O production via nitrification and/or denitrification at low O_2 concentrations. In the brine pool waters, N_2O concentrations were still detectable and remarkably uniform, most likely due to mixing and diffusion of N_2O rather than in-situ production or consumption.

Our results indicate that the Red Sea and the Gulf of Aqaba are unique natural laboratories to study N_2O production and consumption pathways in one of the warmest and most saline regions of the global ocean. We suggest that future investigations of the nitrogen cycle in the Red Sea and Gulf of Aqaba basins should include time series measurements of N_2O concentrations, the associated microbial processes and meso- and submesoscale circulation patterns. To improve our understanding of the N_2O pathways and its emissions to/uptake from the atmosphere, it is critical to (i) decipher the seasonality and interannual variability of N_2O concentrations and (ii) identify the major N_2O production and consumption pathways and their interplay with eddies and
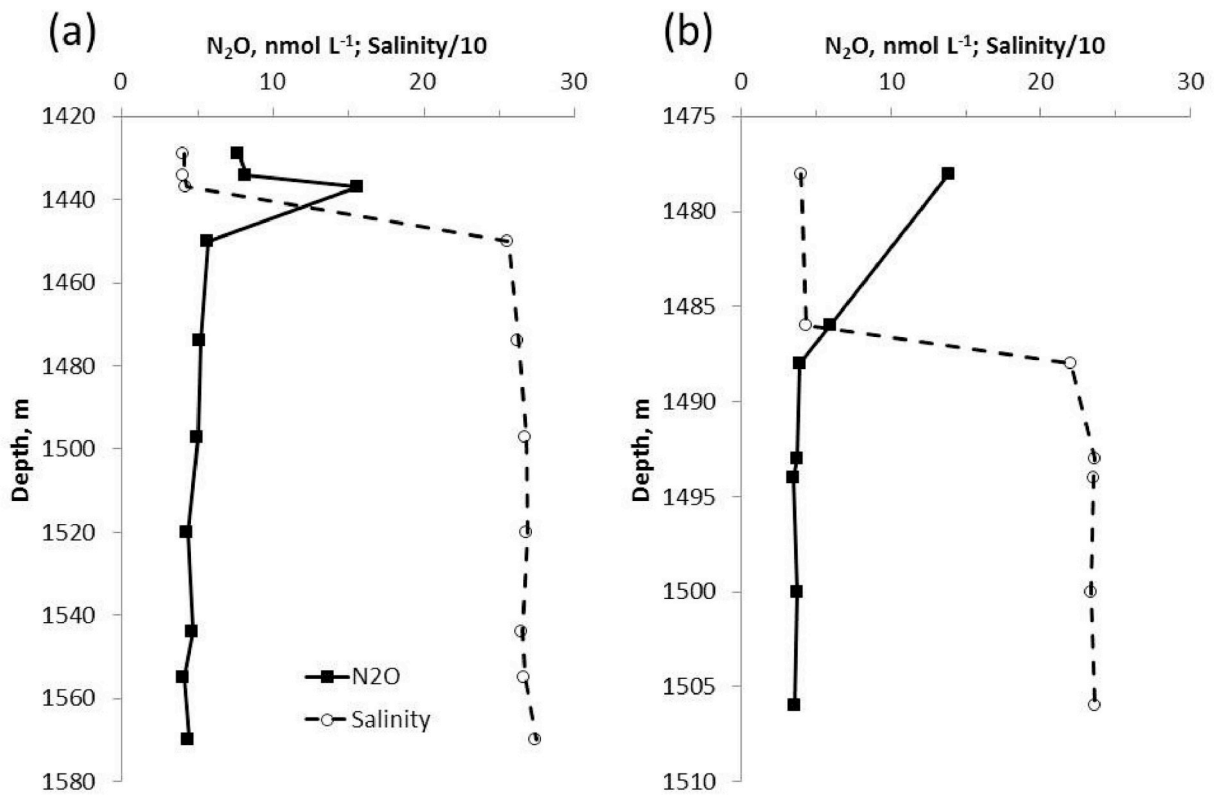
Fig. 12. N_2O concentration profiles of the brine pools in the (a) Oceanographer and (b) Conrad Deeps. Please note that the salinity values were divided by 10 for scaling purposes.
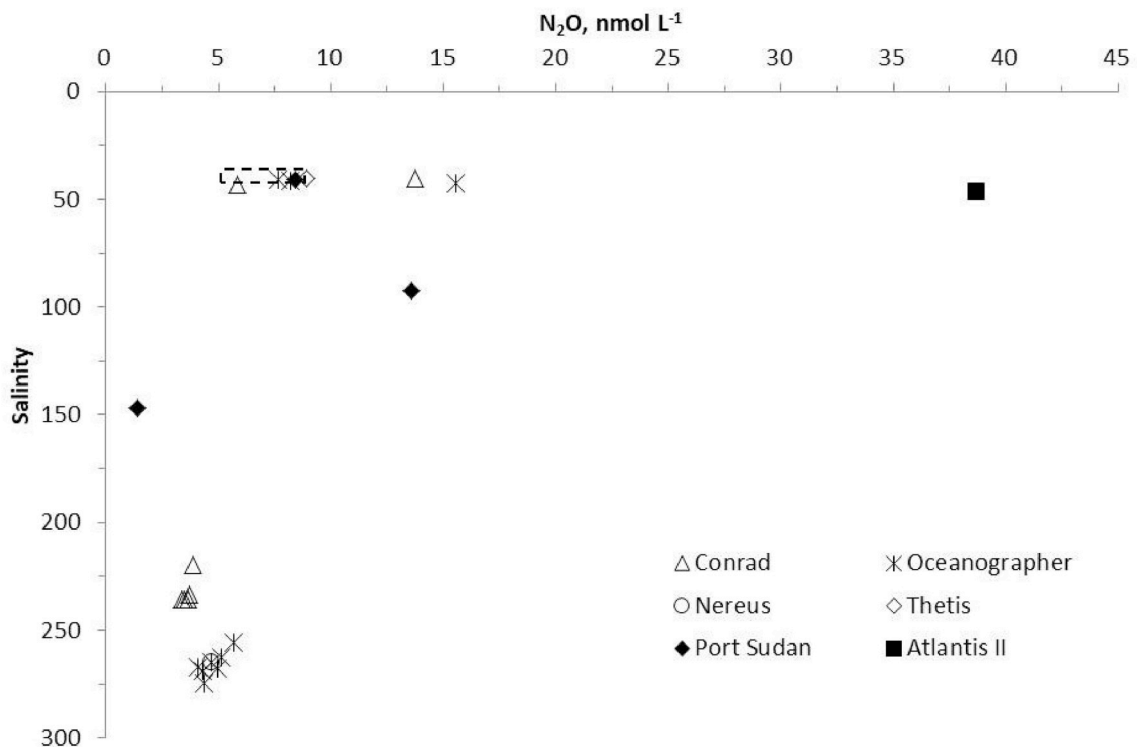
Fig. 13. N_2O concentrations in Red Sea deeps vs. salinity. The open rectangle marks the range of N_2O deep water (> 1500 m) concentrations in 2014 and 2016. Data from the RS05 (January 2005) and NC5 (August 2016) cruises are marked with open and filled symbols, respectively.

filaments. This may provide insights into future N₂O and nitrogen cycling in tropical oceans affected by the ongoing ocean warming.

References

Anderson, B., Bartlett, K., Frolking, S., Hayhoe, K., Jenkins, J., Salas, W., 2010. Methane and Nitrous Oxide Emissions from Natural Sources. (Washington DC).

Anschutz, P., Blanc, G., 1996. Heat and salt fluxes in the Atlantis II deep (Red Sea). Earth Planet. Sci. Lett. 142, 147–159.

Anschutz, P., Blanc, G., Chatin, F., Geiller, M., Pierret, M.C., 1999. Hydrographic changes during 20 years in the brine-filled basins of the Red Sea. Deep-Sea Res. Part I Oceanogr. Res. Pap. 46, 1779–1792.

Antunes, A., Ngugi, D.K., Stingl, U., 2011. Microbiology of the Red Sea (and other) deep-sea anoxic brine lakes. Environ. Microbiol. Rep. 3, 416–433.

Bakker, D.C.E., Bange, H.W., Gruber, N., Johannessen, T., Upstill-Goddard, R.C., Borges, A.V., Delille, B., Löscher, C.R., Naqvi, S.W.A., Omar, A.M., Santana-Casiano, J.M., 2014. Air-sea interactions of natural long-lived greenhouse gases (CO2, N2O, CH4) in a changing climate. In: Liss, P.S., Johnson, M.T. (Eds.), Ocean-Atmosphere Interactions of Gases and Particles. Springer, Heidelberg, pp. 113–169.

Bange, H.W., 2008. Gaseous nitrogen compounds (NO, N₂O, N₂, NH₃) in the ocean. In: Capone, D.G., Bronk, D.A., Mulholland, M.R., Carpenter, E.J. (Eds.), Nitrogen in the Marine Environment, second ed. Elsevier, Amsterdam, pp. 51–94.

Bange, H.W., Freing, A., Kock, A., Löscher, C.R., 2010. Marine pathways to nitrous oxide. In: Smith, K. (Ed.), Nitrous Oxide and Climate Change. Earthscan, London, pp. 36–62.

Bange, H.W., Rapsomanikis, S., Andreae, M.O., 2001. Nitrous oxide cycling in the Arabian Sea. J. Geophys. Res. 106, 1053–1065.

Biton, E., Gildor, H., 2011. The general circulation of the Gulf of Aqaba (Gulf of Eilat) revisited: the interplay between the exchange flow through the 'Straits of Tiran and surface fluxes. J. Geophys. Res.-Oceans 116.

Bonatti, E., Bortoluzzi, G., Calafato, A., Cipriani, A., Ferrante, V., Ligi, M., Lopez Correa, M., Redini, F., Barabino, G., Carminati, E., Mitchell, N., Sichler, B., Schmidt, M., Schmitt Rasul, N., Al Nomani, S., Bahareth, F., Khalil, S., Farawati, R., Gitto, D., Raspagliosi, M., 2005. ISMAR Bologna Technical Report No. 94: Geophysical, Geological and Oceanographic Surveys in the Northern Red Sea. Report on the Morphobathymetric, Magnetometric, Oceanographic, Coring and Dredging Investigations during Cruise RS05 Aboard R/V Urania. Nationla Research Council of Italy, Institute of Marine Sciences, Marine Geology Section (Bologna), Bologna, pp. 40.

Böttger-Schnack, R., Schnack, D., 1989. Vertical distribution and population structure of macrostella gracilis (copepoda: harpacticoida) in the Red Sea in relation to the occurrence of oscillatoria (*Trichodesmium*) spp. (cynaobacteria). Mar. Ecol. Prog. Ser. 52, 17–31.

Cao, H.L., Zhang, W.P., Wang, Y., Qian, P.Y., 2015. Microbial community changes along the active seepage site of one cold seep in the Red Sea. Front. Microbiol. 6.

Carton, J.A., Chao, Y., 1999. Caribbean Sea eddies inferred from TOPEX/POSEIDON altimetry and a 1/6 degrees Atlantic Ocean model simulation. J. Geophys. Res.-Oceans 104, 7743–7752.

Carvalho, S., Kürten, B., Krokos, G., Hoteit, I., Ellis, J., 2019. Chapter 3 - the Red Sea. In: Sheppard, C. (Ed.), World Seas: an Environmental Evaluation, second ed. Academic Press, pp. 49–74.

Coates, C.J., Wyman, M., 2017. A denitrifying community associated with a major, marine nitrogen fixer. Environ. Microbiol. 19, 4978–4992.

Cornejo, M., Farías, L., 2012. Following the N₂O consumpion in the oxygen minimum zone of the eastern South Pacific. Biogeosciences 9, 3205–3212.

Cornejo, M., Murillo, A., Farías, L., 2015. An unaccounted for N₂O sink in the surface water of the eastern subtropical South Pacific ocean: physical versus biological mechanisms. Prog. Oceanogr. 137, 12–23.

David, H.A., 1951. Further applications of range to analysis of variance. Biometrika 38, 393–409.

Devol, A.H., 2008. Denitrification including anammox. In: Capone, D.G., Bronk, D.A., Mulholland, M.R., Carpenter, E.J. (Eds.), Nitrogen in the Marine Environment, second ed. Elsevier, Amsterdam, pp. 263–301.

Eder, W., Jahnke, L.L., Schmidt, M., Huber, R., 2001. Microbial diversity of the brine-seawater interface of the Kebrit Deep, Red Sea, studied via 16S rRNA gene sequences and cultivation methods. Appl. Environ. Microbiol. 67, 3077–3085.

Eder, W., Schmidt, M., Koch, M., Garbe-Schonberg, D., Huber, R., 2002. Prokaryotic phylogenetic diversity and corresponding geochemical data of the brine-seawater interface of the Shaban Deep, Red Sea. Environ. Microbiol. 4, 758–763.

Farías, L., Faúndez, J., Fernandéz, C., Cornejo, M., Sanhueza, S., Carrasco, C., 2013. Biological N₂O fixation in the eastern South Pacific ocean and marine cynaobacterial cultures. PLoS One 8, e63956.

Freing, A., Wallace, D.W.R., Bange, H.W., 2012. Global oceanic production of nitrous oxide. Phil. Trans. R. Soc. B 367, 1245–1255.

Garcias-Bonet, N., Fusi, M., Ali, M., Shaw, D.R., Saikaly, P.E., Daffonchio, D., Duarte, C.M., 2018. High denitrification and anaerobic ammonium oxidation contributes to net nitrogen loss in a seagrass ecosystem in the central Red Sea. Biogeosciences 15, 7333–7346.

Grasshoff, K., Kremling, K., Ehrhardt, M., 1999. Methods of Seawater Analysis, third ed. Wiley-VCH, New York.

Halim, Y., 1969. Plankton of the Red Sea. Oceanogr. Mar. Biol. Annu. Rev. 7, 231–275.

Hartmann, M., Scholten, J.C., Stoffers, P., Wehner, F., 1998. Hydrographic structure of brine-filled deeps in the Red Sea - new results from the Shaban, Kebrit, Atlantis II, and Discovery Deep. Mar. Geol. 144, 311–330.

IPCC, 2013. In: Stocker, T.F., Qin, D., Plattner, G.-K., Tignor, M., Allen, S.K., Boschung, J., Nauels, A., Xia, Y., Bex, V., Midgley, P.M. (Eds.), Climate Change 2013: the Physical Science Basis. Contribution of Working Group I to the Fifth Assessment Report of the Intergovernmental Panel on Climate Change. Cambridge University Press, Cambridge UK and New York, NY, USA, pp. 1535.

Ishijima, K., Sugawara, S., Kawamura, K., Hashida, G., Morimoto, S., Murayama, S., Aoki, S., Nakazawa, T., 2007. Temporal variations of the atmospheric nitrous oxide concentration and its delta N-15 and delta O-18 for the latter half of the 20th century reconstructed from firn air analyses. J. Geophys. Res. Atmos. 112.

Jean-Baptiste, P., Fourre, E., Metzl, N., Ternon, J.F., Poisson, A., 2004. Red Sea deep water circulation and ventilation rate deduced from the He-3 and C-14 tracer fields. J. Mar. Syst. 48, 37–50.

Ji, Q.X., Babbin, A.R., Jayakumar, A., Oleynik, S., Ward, B.B., 2015. Nitrous oxide production by nitrification and denitrification in the Eastern Tropical South Pacific oxygen minimum zone. Geophys. Res. Lett. 42, 10755–10764.

Khalil, A.S.M., 2015. Mangroves of the Red Sea. In: Rasul, N.M.A., Stewart, I.C.F. (Eds.), The Red Sea. Springer-Verlag, Berlin, pp. 585–597.

Kock, A., Arévalo-Martínez, D.L., Löscher, C.R., Bange, H.W., 2016. Extreme N₂O accumulation in the coastal oxygen minimum zone off Peru. Biogeosciences 13, 827–840.

Kubryakov, A.A., Stanichny, S., 2015. Seasonal and interannual variability of the Black Sea eddies and its dependence on characteristics of the large-scale circulation. Deep-Sea Res. Part I Oceanogr. Res. Pap. 97, 80–91.

Kürten, B., Zarokanellos, N.D., Devassy, R.P., El-Sherbiny, M.M., Struck, U., Capone, D.G., Schulz, I.K., Al-Aidaroos, A.M., Irigoien, X., Jones, B.H., 2019. Seasonal modulation of mesoscale processes alters nutrient availability and plankton communities in the Red Sea. Prog. Oceanogr. 173, 238–255.

Le Hénaff, M., Kourafalou, V.H., Morel, Y., Srinivasan, A., 2012. Simulating the dynamics and intensification of cyclonic loop current frontal eddies in the Gulf of Mexico. J. Geophys. Res.-Oceans 117.

Mackey, K.R.M., Bristow, L., Parks, D.R., Altabet, M.A., Post, A.F., Paytan, A., 2011. The influence of light on nitrogen cycling and the primary nitrite maximum in a seasonally stratified sea. Prog. Oceanogr. 91, 545–560.

Maher, D.T., Sippo, J.Z., Tait, D.R., Holloway, C., Santos, I.R., 2016. Pristine mangrove creek waters are a sink of nitrous oxide. Sci. Rep. 6.

Manasrah, R., Raheed, M., Badran, M.I., 2006. Relationships between water temperature, nutrients and dissolved oxygen in the northern Gulf of Aqaba, Red Sea. Oceanologia 48, 237–253.

Meeder, E., Mackey, K.R.M., Paytan, A., Shaked, Y., Iluz, D., Stambler, N., Rivlin, T., Post, A.F., Lazar, B., 2012. Nitrite dynamics in the open ocean - clues from seasonal and diurnal variations. Mar. Ecol. Prog. Ser. 453, 11.

Naqvi, S.W.A., Hansen, H.P., Kureishy, T.W., 1986. Nutrient uptake and regeneration ratios in the Red Sea with references to the nutrient budgets. Oceanol. Acta 9, 271–277.

Nevison, C., Butler, J.H., Elkins, J.W., 2003. Global distribution of N₂O and ΔN₂O-AOU yield in the subsurface ocean. Glob. Biogeochem. Cycles 17, 1119 doi:1110.1029/2003GB002068.

Ngugi, D.K., Blom, J., Alam, I., Rashid, M., Ba-Alawi, W., Zhang, G.S., Hikmawan, T., Guan, Y., Antunes, A., Siam, R., El Dorry, H., Bajic, V., Stingl, U., 2015. Comparative genomics reveals adaptations of a halotolerant thaumarchaeon in the interfaces of brine pools in the Red Sea. ISME J. 9, 396–411.

Orif, M.I., Kavil, Y.N., Kelassanthodi, R., Al-Farawati, R., Al Zobidi, M.I., 2017. Dissolved methane and oxygen depletion in the two coastal lagoons, Red Sea. Indian J. Geo-Mar. Sci. 46, 1287–1297.

Osman, E.O., Smith, D.J., Ziegler, M., Kurten, B., Conrad, C., El-Haddad, K.M., Voolstra, C.R., Suggett, D.J., 2018. Thermal refugia against coral bleaching throughout the northern Red Sea. Glob. Chang. Biol. 24, E474–E484.

Pelz, N., 2017. Verteilung von Lachgas (N₂O) im Roten Meer. University of Hildesheim, Hildesheim, pp. 32.

Pena-Garcia, D., Ladwig, N., Turki, A.J., Mudarris, M.S., 2014. Input and dispersion of nutrients from the Jeddah metropolitan area, Red Sea. Mar. Pollut. Bull. 80, 41–51.

Qurban, M.A., Balala, A.C., Kumar, S., Bhavya, P.S., Wafar, M., 2014. Primary production in the northern Red Sea. J. Mar. Syst. 132, 75–82.

Qurban, M.A., Wafar, M., Jyothibabu, R., Manikandan, K.P., 2017. Patterns of primary production in the Red Sea. J. Mar. Syst. 169, 87–98.

Raes, E.J., Bodrossy, L., de Kamp, J.V., Holmes, B., Hardman-Mountford, N., Thompson, P.A., McInnes, A.S., Waite, A.M., 2016. Reduction of the powerful greenhouse gas N₂O in the south-eastern Indian ocean. PLoS One 11.

Rahav, E., Bar-Zeev, E., Ohayon, S., Elifantz, H., Belkin, N., Herut, B., Mulholland, M.R., Berman-Frank, I., 2013. Dinitrogen fixation in aphotic oxygenated marine environments. Front. Microbiol. 4.

Raitsos, D.E., Brewin, R.J.W., Zhan, P., Dreano, D., Pradhan, Y., Nanninga, G.B., Hoteit, I., 2017. Sensing coral reef connectivity pathways from space. Sci. Rep. 7.

Raitsos, D.E., Pradhan, Y., Brewin, R.J.W., Stenchikov, G., Hoteit, I., 2013. Remote sensing the phytoplankton seasonal succession of the Red Sea. PLoS One 8.

Raitsos, D.E., Yi, X., Platt, T., Racault, M.F., Brewin, R.J.W., Pradhan, Y., Papadopoulos, V.P., Sathyendranath, S., Hoteit, I., 2015. Monsoon oscillations regulate fertility of the Red Sea. Geophys. Res. Lett. 42, 855–862.

Rasul, N.M.A., Nawab, Z.A., Stewart, I.C.F., 2015. Introduction to the Red Sea: its origin, structure, and environment. In: Rasul, N.M.A., Stewart, I.C.F. (Eds.), The Red Sea. Springer Verlag, Heidelberg, pp. 1–28.

Santoso, A., McPhaden, M.J., Cai, W.J., 2017. The defining characteristics of ENSO extremes and the strong 2015/2016 El nino. Rev. Geophys. 55, 1079–1129.

Schmidt, M., Al-Farawati, R., Botz, R., 2015. Geochemical classification of brine-filled Red Sea deeps. In: Rasul, N.M.A., Stewart, I.C.F. (Eds.), The Red Sea. Springer Verlag, Heidelberg, pp. 219–233.

Schmidt, M., Botz, R., Faber, E., Schmitt, M., Poggenburg, J., Garbe-Schönberg, D., Stoffers, P., 2003. High-resolution methane profiles across anoxic brine-seawater boundaries in the Atlantis-II, Discovery, and Kebrit Deeps (Red Sea). Chem. Geol. 200, 359–375.

Sofianos, S., Johns, W.E., 2015. Water mass formation, overturning circulation, and the exchange of the Red Sea with the adjacent basins. In: Rasul, N.M.A., Stewart, I.C.F. (Eds.), The Red Sea. Springer Verlag, Heidelberg, pp. 343–353.

Sun, X., Jayakumar, A., Ward, B.B., 2017. Community composition of nitrous oxide consuming bacteria in the oxygen minimum zone of the eastern tropical South pacific. Front. Microbiol. 8.

Swift, S.A., Bower, A.S., Schmitt, R.W., 2012. Vertical, horizontal, and temporal changes in temperature in the Atlantis II and Discovery hot brine pools, Red Sea. Deep-Sea Res. Part I Oceanogr. Res. Pap. 64, 118–128.

Torregrosa-Crespo, J., Pire, C., Martínez-Espinosa, R.M., Bergaust, L., 2019. Denitrifying haloarchaea within the genus Haloferax display divergent respiratory phenotypes, with implications for their release of nitrogenous gases. Environ. Microbiol. 21, 427–436.

Wafar, M., Qurban, M.A., Ashraf, M., Manikandan, K.P., Flandez, A.V., Balala, A.C., 2016. Patterns of distribution of inorganic nutrients in Red Sea and their implications to primary production. J. Mar. Syst. 156, 86–98.

Walter, S., Bange, H.W., Breitenbach, U., Wallace, D.W.R., 2006a. Nitrous oxide in the North Atlantic Ocean. Biogeosciences 3, 607–619.

Walter, S., Breitenbach, U., Bange, H.W., Nausch, G., Wallace, D.W.R., 2006b. Distribution of N₂O in the Baltic Sea during transition from anoxic to oxic conditions. Biogeosciences 3, 557–570.

Ward, B.B., 2008. Nitrification in marine systems. In: Capone, D.G., Bronk, D.A., Mulholland, M.R., Carpenter, E.J. (Eds.), Nitrogen in the Marine Environment, second ed. Elsevier, Amsterdam, pp. 199–261.

Weiss, R.F., 1970. The solubility of nitrogen, oxygen and argon in water and seawater. Deep-Sea Res. 17, 721–735.

Weiss, R.F., Price, B.A., 1980. Nitrous oxide solubility in water and seawater. Mar. Chem. 8, 347–359.

Weiss, R.F., Van Woy, F.A., Salameh, P.K., 1992. Surface Water and Atmospheric Carbon Dioxide and Nitrous Oxide Observations by Shipboard Automated Gas Chromatography: Results from Expeditions between 1977 and 1990. Carbon Dioxide Information Analysis Center. Oak Ridge National Laboratory, Oak Ridge, Tennessee, pp. 144.

Westley, M.B., Yamagishi, H., Popp, B.N., Yoshida, N., 2006. Nitrous oxide cycling in the Black Sea inferred from stable isotope and isotopomer distributions. Deep-Sea Res. Part II 53, 1802–1816.

Wickham, S.A., Claessens, M., Post, A.F., 2015. Ciliates, microbes and nutrients: interactions in the seasonally mixed Gulf of Aqaba. J. Plankton Res. 37, 258–271.

Winkler, L.W., 1888. Die Bestimmung des im Wasser gelösten Sauerstoffes. Ber. Dtsch. Chem. Ges. 21, 2843–2854.

WMO, 2014. In: WMO (Ed.), Scientific Assessment of Ozone Depletion, pp. 416 Geneva, Switzerland.

Wolf-Vecht, A., Paldor, N., Brenner, S., 1992. Hydrographic indications of advection/convection effects in the Gulf of Elat. Deep-Sea Res. Part a-Oceanographic Research Papers 39, 1393–1401.

Yoshinari, T., 1976. Nitrous oxide in the sea. Mar. Chem. 4, 189–202.

Zamora, L.M., Oschlies, A., Bange, H.W., Huebert, K.B., Craig, J.D., Kock, A., Löscher, C.R., 2012. Nitrous oxide dynamics in low oxygen regions of the Pacific: insights from the MEMENTO database. Biogeosciences 9, 5007–5022.

Zarokanellos, N.D., Papadopoulos, V.P., Sofianos, S.S., Jones, B.H., 2017. Physical and biological characteristics of the winter-summer transition in the Central Red Sea. J. Geophys. Res.-Oceans 122, 6355–6370.

Zhan, P., Subramanian, A.C., Yao, F.C., Hoteit, I., 2014. Eddies in the Red Sea: a statistical and dynamical study. J. Geophys. Res.-Oceans 119, 3909–3925.